Influence of mechanical attrition treatment on 17-4PH stainless steel: comparison at sub-micron scale between sent specimens produced by atomic diffusion additive manufacturing (ADAM) process

Claire Gong, Joseph Marae Djouda, Abdelhamid Hmima, Fabrice Gaslain, Thomas Maurer, Benoît Panicaud, Mahdi Chemkhi

INFLUENCE OF MECHANICAL ATTRITION TREATMENT ON 17-4PH STAINLESS STEEL: COMPARISON AT SUB-MICRON SCALE BETWEEN SENT SPECIMENS PRODUCED BY ATOMIC DIFFUSION ADDITIVE MANUFACTURING (ADAM) PROCESS

Claire Gong[a,*], Joseph Marae Djouda[b,c], Abdelhamid Hmima[a], Fabrice Gaslain[d], Mahdi Chemkhi[b,e], Thomas Maurer[a], Benoît Panicaud[e]

[a]*Light, Nanomaterials, Nanotechnologies, CNRS EMR 7004, University of Technology of Troyes, Troyes, France*
[b]*EPF Graduate School of Engineering, 2 rue Fernand Sastre, 10430 Rosières-Prés-Troyes, France*
[c]*Université Paris-Saclay, ENS Paris-Saclay, CNRS, LMT – Laboratoire de Mécanique et Technologie, Gif-sur-Yvette, France*
[d]*MINES ParisTech, PSL - Research University, Centre des Matériaux CNRS UMR 7633, Evry, France*
[e]*Life Assessment of Structures, Materials, mechanics and Integrated Systems, University of Technology of Troyes, Troyes, France*

ABSTRACT

This study focuses on the comparison between two types of single edge notched tensile (SENT) specimens made by Atomic Diffusion Additive Manufacturing (ADAM) process from Markforged Inc. The first type is submitted to Surface Mechanical Attrition Treatment (SMAT) and the second specimens are as fabricated. The deposition of gold nanoparticles (NP) at the surface, through Electron Beam Lithography (EBL), allows characterization at sub-micron scale. To observe the crack initiation and propagation, an in-situ tensile test if performed under scanning electron microscope (SEM) in order to track the NP displacements and the cracks evolution.

Keywords: Nanogauges gratings; 2D characterization; Additive manufacturing; SMAT; crack propagation;

---

1. Introduction

The potential of additive manufacturing (AM) in the industrial field has led to multiple improvements over the last decade. The main advantages of such technic are the cost-effectiveness and the liberty of design [1]. The layer-by-layer build-up process allows the emergence of a variety of technics: fused filament fabrication, selective laser melting, direct energy deposition... Moreover, the material used for this type of fabrication can be chosen conveniently. Started with thermoplastic materials, it is now possible to print metallic and ceramic parts [2][3].

Many companies offer different methods to facilitate the democratization of AM but one of the most convenient methods is the Material Extrusion Additive Manufacturing (MEAM). For metallic materials, the feedstock is a filament made by a mix between the metallic powder and a polymerous binder, which is heated and extruded through a nozzle [4]. However, as any other materials made by AM, the mechanical properties are altered by the manufacturing process. Generally speaking, a bonding issue between the layers or the presence of porosity can be observed [4][5].

* Corresponding author: claire.gong@utt.fr

In this context, different post-treatment technics are required and can therefore be applied in order to enhance the microstructures characteristics, thus improving the macroscopic behavior. To compare the results of such treatments, it is possible to observe their influence at a local scale, especially on crack initiation and propagation, under a mechanical testing.
Surface Mechanical Attrition Treatment (SMAT) is a post-treatment used to create a nanocristallized layer at the surface, increasing the hardness and improving the mechanical properties [6]. In order to quantify the difference and to compare the progression of crack propagation, a grating of nanoparticles (NP) is deposited near the tip of single edge notched samples through Electron-Beam Lithography (EBL). The displacements of the NP, captured by scanning electron microscope (SEM) imaging, enable to obtain strain mappings and therefore, to have quantitative information at a local scale.

Based on previous studies [7][8], the EBL process for this purpose is quite well-known. In this study, the stainless steel 17-4PH is used for the fabrication of the samples, a ferrous-chromium steel appreciated for its high strength and resistance to corrosion [9].

2. Method

2.1. Sample's preparation

The Atomic Diffusion Additive Manufacturing (ADAM) technic from Markforged Inc. is based on the material extrusion additive manufacturing (MEAM) process: a thermoplastic binder is mixed with the metallic powder into a filament. The filament is then extruded with a heated nozzle to build, layer by layer, the requested part. The as-printed piece is placed into a solvent to remove the majority of the binder. The final step consists in sintering the part near its melting point, in order to dispose of the binder and to fuse the metallic powder into a relatively dense metallic material [4].

Four single edge notched tension (SENT) specimens were fabricated, with a width of 250 µm and a layer of 50 µm for the post-sintered filament. The dimensions of the samples are indicated in Fig. 1 (a) and the orientation of the filling is inclined by a 45° angle, see Fig. 1 (b). The ASTM E1820 standard and the NF EN ISO 6892-1 standard were used as a guide to create the different dimensions.

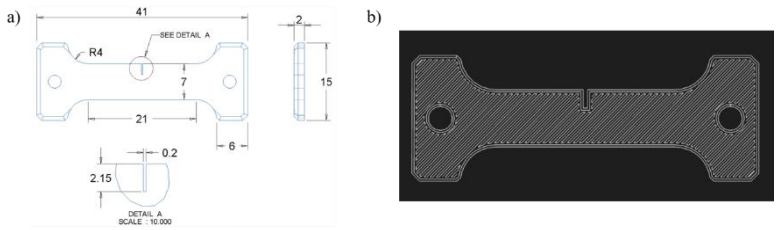

Fig. 1. (a) Drawing of SENT part in millimeters; (b) Orientation of the nozzle during the printing step (45°/-45°).

To prepare the samples for EBL and NP deposition, it is necessary to have a mechanical polishing on the studied surface in order to decrease the roughness of the material. A diamond paste of 1 µm is the last step before obtaining a mirror finish.

Since the maximum load for the tensile test machine is 5 kN, the thickness of the specimens must be near 1.2 mm in order to obtain a crack initiation and to conduct the tensile test until the failure of the material.

All four 17-4PH parts were mirror polished, and two specimens were submitted to a SMAT treatment afterwards. This variant of shot-peening introduces different conditions: a closed environment, bigger shot size which strike randomly the surface with a lower velocity imposed by a sonotrode [10]. The severe plastic deformation created by the shot impacts lead to increase the micro-hardness and improve mechanical properties but multiple parameters can have an influence on the results. For this study, one of the main concern about this mechanical treatment

is to obtain the lowest roughness. Therefore, the chosen conditions are in accordance to a SMAT high: the duration of the treatment is 30 minutes, with 3 mm shots diameter at 20 kHz frequency for the sonotrode. After SMAT, the average roughness Ra is around 0.47 µm for the studied surface.

In order to avoid any confusion, the as-fabricated mirror polished samples will be named AF sample 1 and AF sample 2 and the two SMATed samples will be designated as SMATed sample 1 and SMATed sample 2.

2.2. Nanogauges deposition

The EBL process is composed by a few steps: following the mechanical polishing as explained before, the prepared surface is then coated with a polymethyl methacrylate (PMMA) resin. An electron beam focuses on areas of interest defined by the user. The exposition to the beam weakens the resin, allowing to remove the PMMA with only a chemical solvent, composed by methyl isobutyl ketone and isopropyl alcohol solutions: it is the development step. After the exposed resin has been removed, a layer of gold NP is deposited at the surface, covering the resin but also the initial substrate. Gold is a widespread material involved in nanofabrication process, ensuring a good contrast during SEM observation thanks to its conductive properties [11]. The final step, called lift-off, consists of putting the sample in an solvent to definitely remove the rest of the resin and to only keep the NP on the substrate.

Even if the deposition process is known, the main concern about the following of crack initiation and propagation is to predict the location of the cracks. In this study, a large grating has been implemented to confirm the complete coverage near the tip of the notch. The electron beam exposition was conducted under a Raith e-LiNE Electron Beam Lithography, the entire nanogauge design is a 400 x 400 µm² grating divided by sixteen 100 x100 µm² subgratings. Each of these subgratings has a contour of different 1 µm geometric shapes (circles, triangles, squares and semi-circles) in order to obtain a better tracking of the crack propagation during the tensile test and to differentiate each subgrating during the SEM observation and imaging.

The dimensions of the NP follows previous tests [8][12], ensuring a satisfying spatial resolution and a clear distinction between the NP.

Each NP has a diameter of 200 nm, a height of 50 nm and a distance between centers of 400 nm. The four samples present distinguishable results regarding their depositions, see Fig. 2.

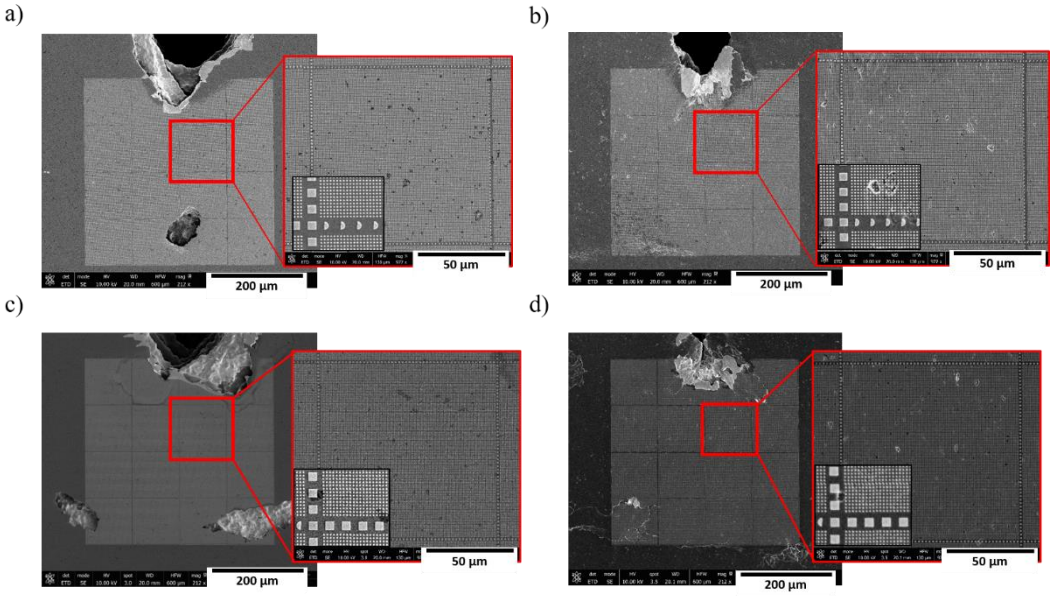

Fig. 2. Gratings deposition with magnification at initial state for (a) AF sample 1; (b) SMATed sample 1; (c) AF sample 2; (d) SMATed sample 2.

2.3. In-situ tensile test setup

The FEI Nova NanoSEM 450 was used for the in-situ tensile test. The setup for each test is presented in Fig. 3 (a). To ensure a good resolution in order to distinguish all NP, the SEM can take several seconds to record the images. Therefore, the loading must be paused frequently, every 125 N, to save the whole grating with a horizontal field width (HFW) of 600 µm but also each subgrating containing all NP with a HFW of 130 µm. The images have a resolution of 4096 x 3775 pixels.

Before the beginning of the loading, a number is attributed to each subgratings to avoid any confusion during the test, See Fig. 3 (b).

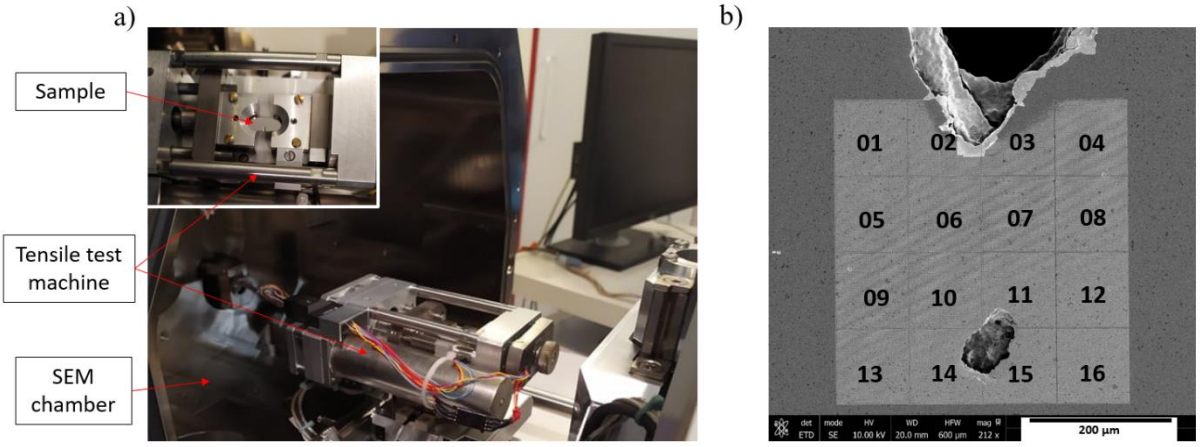

Fig. 3. (a) Setup for the in-situ tensile test under the SEM; (b) The assigned numbers to identify each subgrating.

3. Results and discussion

3.1. Macroscopic results

Following the four tests, a macroscopic stress-strain curve has been plotted for each specimen and presented in Fig. 4.

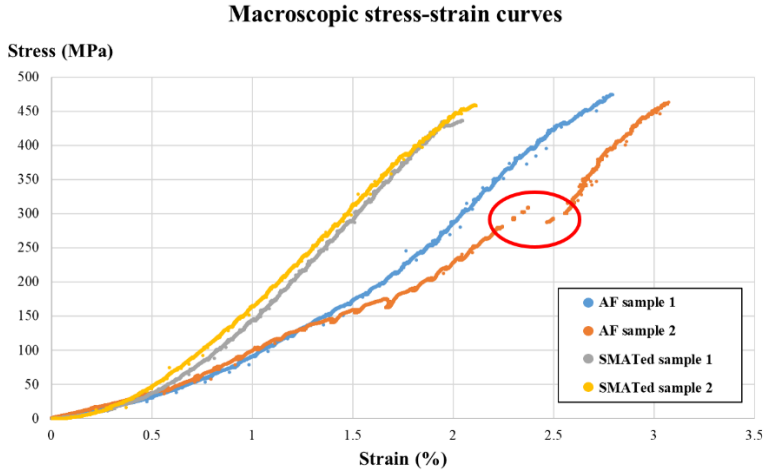

Fig. 4. Macroscopic stress-strain curves.

The macroscopic curves can show a reproducibility in the results and enable a comparison of the post-treatment influence. The two curves belonging to the SMATed samples have a greater rigidity. At 1.5 % of macroscopic strain, the AF samples 1 has a 173 MPa stress and the AF sample 2 is around 159 MPa, while the SMATed samples 1 and 2 are respectively at 290 MPa

and at 312 MPa. Moreover, the final elongation is lower for the treated specimens, where both samples break around 2 %, while the AF samples break at 2.79 % and at 3.07 %.

The particular noise showed by the curves can be explained by the discontinuity of the experiment, when it was planned to pause the tests frequently to obtain SEM images. However, the important disruption in the middle of the AF sample 2 around 2.5 % and circled in red in Fig. 4, is due to a technical problem, which occurred during the test. Other tests could be performed in order to validate the general behavior for macroscopic stress-strain curve of the AF samples.

The relevant values for the four samples are detailed in Table 1.

Table 1. Relevant values for the stress-strain curves.

	AF sample 1	AF sample 2	SMATed sample 1	SMATed sample 2
Maximum load *(N)*	3890	3960	3779.5	3852
Maximum elongation *(mm)*	0.488	0.534	0.358	0.37
Ultimate tensile strength *(MPa)*	474.48	463.41	436.48	458.67
Maximum strain *(%)*	2.788	3	2.04	2.1

A stress concentration is present around the notch. Therefore, a concentration factor K_t must be multiplied by the macroscopic load and divided by the section under the notch in order to obtain the local stress. Regarding the specimen's dimensions, K_t is equal to 3 [13]. In the following figures depicting the SEM images, the indicated stress values are the concentrated stress, as it is the value at which the cracks appear.

3.2. Analysis of SEM images for AF samples

By comparing the two AF samples after their tests in Fig. 5, some similarities and differences can be highlighted. For both specimens, the visible cracks appeared at a specific location, where a small portion of a large porosity can be observed near the tip of the notch. The origin of such a porosity may come from the binder, where it is crucial to remove the maximum of the binder in order to avoid the formation of bubble near the surface of the part [14].

Moreover, the number of cracks appearing at the beginning of the test is different. Indeed, as it is shown in Fig. 5 (a), the four black arrows for AF sample 1 exhibits four cracks at the beginning of the test, while the second AF sample has a single crack. This difference can easily be explained by the geometry of the notch's border. Although both samples present an important porosity under the surface, the subgrating 03 of AF sample 1 covers a smooth and circular border, promoting a more balanced distribution of the load applied, whereas for the AF sample 2, a sharper border can be seen on the subgrating number 2.

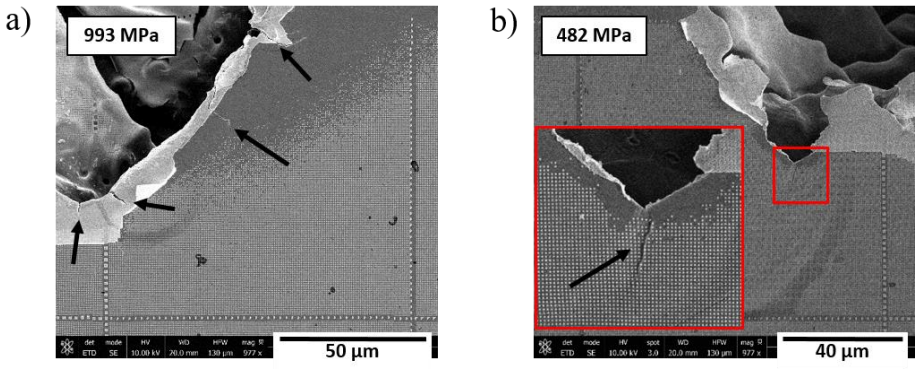

Fig. 5. SEM image of (a) subgrating 03 at 993 MPa for AF sample 1; (b) subgrating 02 at 482 MPa for AF sample 2.

Furthermore, the presence of porosity in AM samples, smaller than the one described previously, is important enough to guide the crack's path during its progression throughout the experiment. The Fig. 6 shows the visible porosity for both samples, at 1752 MPa for AF sample 1 and at 1857 MPa for AF sample 2. The red circles in Fig. 6 highlight these porosities along the path of the crack.

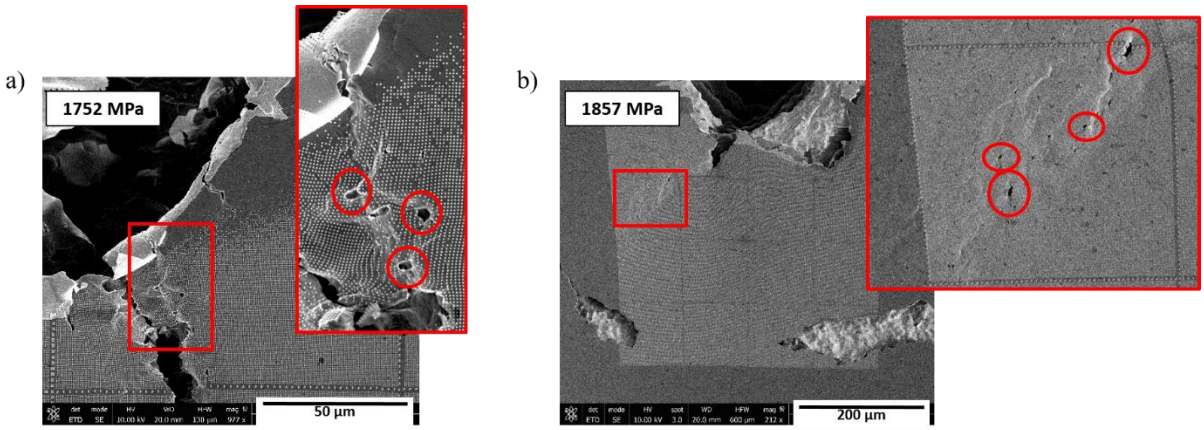

Fig. 6. Magnification of the porosity in the SEM images for (a) AF sample 1; (b) AF sample 2.

3.3. Analysis of SEM images for SMATed samples

The shot impacts and the plastic deformation at the surface of the samples have created a gathering of the material, or overlaps, around the notch, as it can be seen on Fig. 7 (a) and (c) for both SENT specimens at the initial state. Regarding the cracks, an important discontinuity caused by these overlaps around the notch should lead to a stress concentration at their borders. In Fig. 7 (b), two visible cracks are present at 1829 MPa for the SMATed sample 1, where the limits of the two overlaps can be observed. The first crack in SMATed sample 1 appeared at around 1152 MPa and at 1355 MPa for the second crack. Concerning the SMATed sample 2, the first crack is visible at 1481 MPa and the second crack at 1802 MPa. The cracks are showed in an advanced stage in Fig. 7 (b) and (d) in order to guaranty the crack's visibility for both specimens.

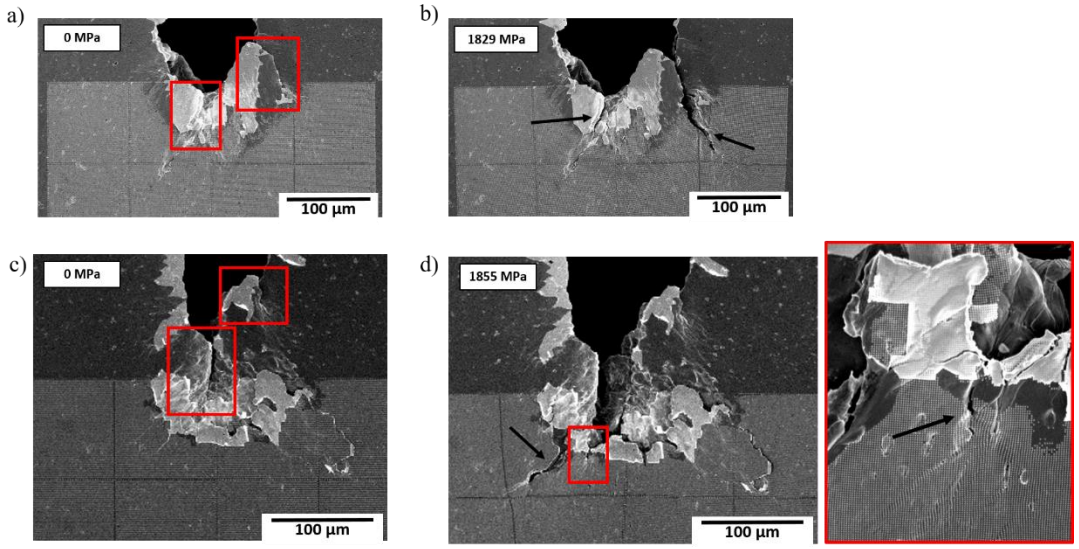

Fig. 7. SEM images of (a) SMATed sample 1 at initial state; (b) SMATed sample 1 at 1829 MPa; (c) SMATed sample 2 at initial state; (d) SMATed sample at 1855 MPa with a magnification zone.

The observations on the AF samples shows the benefits of the SMAT treatment in delaying crack initiation. However, the nanocristallized layer generated after the treatment does not completely cancel the effect of the porosity in the material. Indeed, the magnifications presented in Fig. 8 show some porosity through the path of the second cracks, suggesting that some porosities can still be opened during the tensile test.

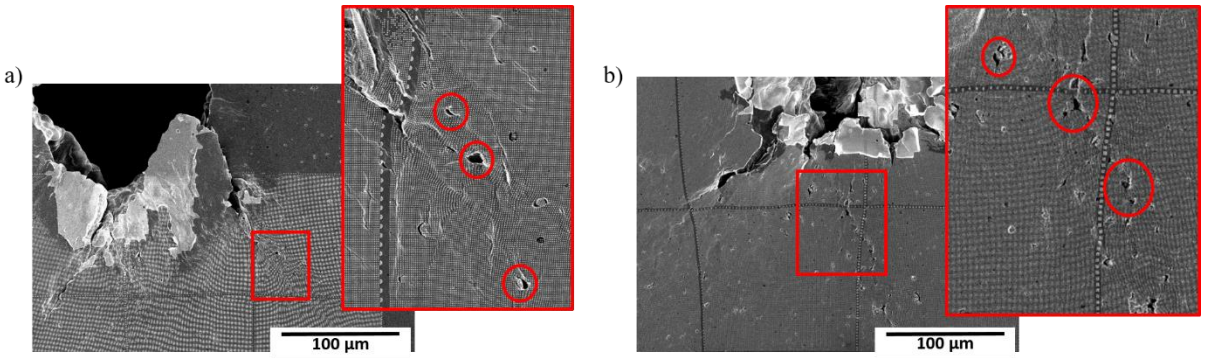

Fig. 8. Magnification of the porosity in the SEM images for (a) SMATed sample 1; (b) SMATed sample 2.

4. Conclusion

The present study highlights the effect of SMAT treatment at sub-micron scale, using a new method to obtain qualitative and quantitative information through SEM observations. This SMAT treatment leads to rigidify the material and creates overlaps over narrow areas. Based on the present observations, the crack's initiation depends strongly on the geometry at the tip of the notch, but also on the presence of porosities near the crack beneath the surface that seem to guide the crack propagation. The amount of information brought by the displacements of the NP can improve the comprehension of the material's behavior at such scale and thus, make possible the optimization of additive manufactured parts.

5. Acknowledgments

This work has been supported by the Agence Nationale de la Recherche and the FEDER (INSOMNIA project, contract ANR-18-CE09-0003). This work has been made within the framework of the Graduate School NANO-PHOT (Ecole Universitaire de Recherche, contract ANR-18-EURE-0013). Financial support of Nano'Mat (www.nanomat.eu) by the "Ministère de l'enseignement supérieur et de la recherche", the "Fonds Européen de Développement Régional" (FEDER), the "Région Grand-Est", and the "Conseil général de l'Aube" are acknowledged. The authors wish to thank the FabAdd platform of EPF Troyes for the fabrication of the specimens.

References

[1] L.Y. Chen, S.X. Liang, Y. Liu, L.C. Zhang, Additive Manufacturing of Metallic Lattice Structures: Unconstrained Design, Accurate Fabrication, Fascinated Performances, and Challenges, Materials Science and Engineering: R: Reports 146 (2021) 100648.
[2] D. Herzog, V. Seyda, E. Wycisk, C. Emmelmann, Additive Manufacturing of Metals, Acta Materialia 117 (2016) 371-392.
[3] Y. Lakhdar, C. Tuck, J. Binner, A. Terry, R. Goodridge, Additive Manufacturing of Advanced Ceramic Materials, Progress in Materials Science 116 (2021) 100736.
[4] J. Gonzalez-Gutierrez, S. Cano, S. Schuschnigg, C. Kukla, J. Sapkota, C. Holzer, Additive Manufacturing of Metallic and Ceramic Components by the Material Extrusion of Highly-Filled Polymers: A Review and Future Perspectives, Materials 11, no 5 (2018) 840.
[5] T. Mukherjee, J. S. Zuback, A. De, T. DebRoy, Printability of Alloys for Additive Manufacturing, Scientific Reports 6, no 1 (2016) 19717.

[6] Q. Portella, M. Chemkhi, D. Retraint, Influence of Surface Mechanical Attrition Treatment (SMAT) Post-Treatment on Microstructural, Mechanical and Tensile Behaviour of Additive Manufactured AISI 316L, Materials Characterization 167 (2020) 110463.
[7] A. Clair, M. Foucault, O. Calonne, Y. Lacroute, L. Markey, M. Salazar, V. Vignal, E. Finot, Strain Mapping near a Triple Junction in Strained Ni-Based Alloy Using EBSD and Biaxial Nanogauges, Acta Materialia 59, no 8 (2011) 3116-3123.
[8] J. Marae Djouda, Y. Madi, F. Gaslain, J. Beal, J. Crépin, G. Montay, L. Le Joncour, N. Recho, B. Panicaud, T. Maurer, Investigation of Nanoscale Strains at the Austenitic Stainless Steel 316L Surface: Coupling between Nanogauges Gratings and EBSD Technique during in Situ Tensile Test, Materials Science and Engineering: A 740 741 (2019) 315-335.
[9] B. Bai, R. Hu, C. Zhang, J. Xue, W. Yang, Effect of Precipitates on Hardening of 17-4PH Martensitic Stainless Steel Serviced at 300 °C in Nuclear Power Plant, Annals of Nuclear Energy 154 (2021) 108123.
[10] D. Gallitelli, D. Retraint, E. Rouhaud, Comparison between Conventional Shot Peening (SP) and Surface Mechanical Attrition Treatment (SMAT) on a Titanium Alloy, Advanced Materials Research 996 (2014) 964-968.
[11] I. Khan, K. Saeed, I. Khan, Nanoparticles: Properties, Applications and Toxicities. Arabian Journal of Chemistry 12 (2017) 908-931.
[12] J. Marae Djouda, G. Montay, B. Panicaud, J. Beal, Y. Madi, T. Maurer, Nanogauges Gratings for Strain Determination at Nanoscale, Mechanics of Materials 114 (2017) 268-278.
[13] W.D. Pilkey, D.F Pilkey, Z. Bi, Peterson's stress concentration factors. In: John Wiley & Sons, second ed., A Wiley-Interscience Publication, New York, 2020, pp. 105.
[14] J. Gonzalez-Gutierrez, D. Godec, C. Kukla, T. Schlauf, C. Burkhardt, C. Holzer, Shaping, debinding and sintering if steel components via fused filament fabrication, 16th International Scientific Conference on Production Engineering - Computer Integrated Manufacturing and High Speed Machining (2017), 7.